JACS
JOURNAL OF THE AMERICAN CHEMICAL SOCIETY

ARTICLE

pubs.acs.org/JACS

A Bronze Matryoshka: The Discrete Intermetalloid Cluster $[Sn@Cu_{12}@Sn_{20}]^{12-}$ in the Ternary Phases $A_{12}Cu_{12}Sn_{21}$ (A = Na, K)

Saskia Stegmaier and Thomas F. Fässler*

Department of Chemistry, Technische Universität München, Lichtenbergstrasse 4, 85747 Garching, Germany

Supporting Information

ABSTRACT: The synthesis and crystal structure of the first ternary A−Cu−Sn intermetallic phases for the heavier alkali metals A = Na to Cs is reported. The title compounds $A_{12}Cu_{12}Sn_{21}$ show discrete 33-atom intermetalloid Cu−Sn clusters $\{Sn@Cu_{12}@Sn_{20}\}$, which are composed of $\{Sn_{20}\}$ pentagonal dodecahedra surrounding $\{Cu_{12}\}$ icosahedra with single Sn atoms at the center. $Na_{12}Cu_{12}Sn_{21}$ and $K_{12}Cu_{12}Sn_{21}$ were characterized by single-crystal XRD studies, and the successful synthesis of analogous A−Cu−Sn compounds with A = Rb and Cs is deduced from powder XRD data. The isotypic $A_{12}Cu_{12}Sn_{21}$ phases crystallize in the cubic space group $Pn\bar{3}m$ (No. 224), with the Cu−Sn clusters adopting a face centered cubic arrangement. A formal charge of 12− can be assigned to the $\{Sn@Cu_{12}@Sn_{20}\}$ cluster unit, and the interpretation of the title compounds as salt-like intermetallic phases featuring discrete anionic intermetalloid $[Sn@Cu_{12}@Sn_{20}]^{12-}$ clusters separated by alkali metal cations is supported by electronic structure calculations. For both $Na_{12}Cu_{12}Sn_{21}$ and $K_{12}Cu_{12}Sn_{21}$, DFT band structure calculations (TB-LMTO-ASA) reveal a band gap. The discrete $[Sn@Cu_{12}@Sn_{20}]^{12-}$ cluster is analyzed in consideration of the molecular orbitals obtained from hybrid DFT calculations (Gaussian 09) for the cluster anion. The $[Sn@Cu_{12}@Sn_{20}]^{12-}$ cluster MOs can be classified with labels indicating the numbers of radial and angular nodes, in the style of spherical shell models of cluster bonding.

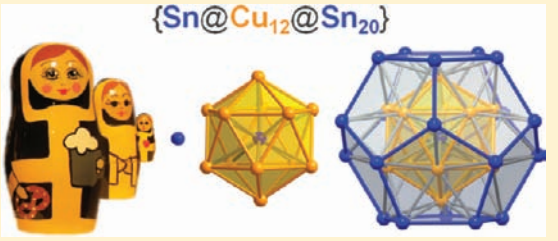

INTRODUCTION

Homo- and heterometallic clusters mark a rendezvous point of gas-phase cluster science, solution-based cluster chemistry, and solid-state chemistry of (semi)metallic elements and intermetallic systems. To describe heterometallic species at that intersection, the term *intermetalloid* cluster has first been coined in view of polyhedral cages of (semi)metal atoms encapsulating another metal atom, especially deltahedral homoatomic group 14 Zintl cluster anions filled with an endohedral late d block metal atom.[1] It was prompted by the previously introduced concept of *metalloid* or elementoid clusters,[2] which was framed for a class of ligand-stabilized clusters as this was joined by a number of Al and Ga clusters. The suffix "oid" was launched to indicate that those clusters show, at a molecular scale, arrangements of metal atoms that relate to the bulk solid-state structures of element modifications. The large metalloid clusters exhibit an assembly of naked metal atoms in the cluster core that is protected by an outer shell that includes ligand-bearing metal atoms. While the protection of the cluster core by a ligand shell is seen as substantial in the concept of metalloid clusters, the term intermetalloid was first used for ligand-free cluster ions. It has been pointed out recently[3] that a comprehensive view of related ligand-stabilized and bare ligand-free clusters is indicated for hetero- as well as for homometallic clusters. The concept of intermetalloid clusters may include both ligand-stabilized and ligand-free cluster species that comprise atoms of at least two different (semi)metallic elements. According to a commonly cited attribute of metalloid clusters, a ligand-stabilized intermetalloid cluster should exhibit more direct metal−metal than metal−ligand contacts.

Following the original motivation for the usage of the suffix "oid" in the term metalloid, a heterometallic cluster addressed as *intermetalloid* ideally bears some structural resemblance to a related intermetallic's solid-state structure. A characteristic structural feature of typical intermetallics (such as Laves phases or Hume−Rothery phases) is the occurrence of high coordination numbers. Thus, clusters with endohedral atoms are seen as exemplary intermetalloid species.[1] Among the ligand-free heterometallic clusters that comprise semi(metallic) p block element atoms, species with endohedral d block atoms constitute one of the prevalent groups. An extensive overview on homo- and heterometallic cluster anions with group 14 and group 15 elements has been given recently.[4] Structurally characterized examples of ligand-free intermetalloid clusters with group 14 element atoms include clusters with one endohedral atom in 9-, 10-, or 12-atom cages, such as $[Ni@Ge_9]^{3-}$, $[Ni@Sn_9]^{3-}$,[5] $[Cu@Sn_9]^{3-}$, $[Cu@Pb_9]^{3-}$, $[Fe@Ge_{10}]^{3-}$, $[Co@Ge_{10}]^{3-}$, $[Ni@Pb_{10}]^{2-}$, $[Ir@Sn_{12}]^{3-}$, $[Ni@Pb_{12}]^{2-}$, $[Pd@Pb_{12}]^{2-}$, and $[Pt@Pb_{12}]^{2-}$, and also larger clusters with 17 or 18 group 14 element atoms and two or even three d block element atoms, such as $[Ni_2@Sn_{17}]^{4-}$, $[Pt_2@Sn_{17}]^{4-}$, $[Pd_2@Ge_{18}]^{4-}$, $[Pd_2@Sn_{18}]^{4-}$, and $[Ni_3@Ge_{18}]^{4-}$.[4] Ligand-free ternary intermetalloid clusters with group 14 and group 15 element atoms and d or f

Received: June 25, 2011
Published: September 30, 2011

block element atoms include $[Eu@Sn_6Bi_8]^{4-}$, $[Ni_2Sn_7Bi_5]^{3-}$,[6] and $[Zn_6Sn_3Bi_8]^{4-}$.[4] Larger ligand-free clusters showing more complex structures were also found for the combination of group 15 element atoms with d block element atoms, for example, $[Pd_7As_{16}]^{4-}$ and $[Ni_5Sb_{17}]^{4-}$, as well as $[Zn@Zn_8Bi_4@Bi_7]^{5-}$ and $[As@Ni_{12}@As_{20}]^{3-}$.[4] All of the ligand-free anionic intermetalloid clusters mentioned above were characterized in salts obtained from reactions of p block element Zintl anions with organometallic d or f block metal compounds.[4] A number of discrete intermetalloid cage clusters with single endohedral d block metal atoms also appear in polar intermetallic phases with group 13 elements (neat solid-state compounds), including $[Zn@E_{10}]^{8-}$ in K_8ZnE_{10} (E = In, Tl), $[Ni@Ga_{10}]^{10-}$ in $Na_{10}NiGa_{10}$, $[M@E_{10}]^{10-}$ in $K_{10}ME_{10}$ (M = Ni, Pd, Pt; E = In, Tl), $[Pd@Tl_{11}]^{8-}$ in A_8PdTl_{11} (A = K, Rb, Cs),[7] and $[M@Tl_{12}]^{12-}$ in $Na_{14}K_6Tl_{18}M$ (M = Zn, Cd, Hg).[8] Also, cationic cage clusters with interstitial atoms are known in case of Bi, $[Pd@Bi_{10}]^{4+}$, for example in $Bi_{14}PdBr_{16}$,[19] and $[Au@Bi_{10}]^{5+}$ in $AuBi_{14-\delta}Sn_{2+\delta}X_{21-\delta}$ ($\delta \approx 0.4$)[10] with X = Cl, Br.

Up to now, the largest ligand-free intermetalloid clusters with p and d block element atoms were obtained from solution-based cluster chemistry. While the largest known cluster $[Au_3Ge_{45}]^{9-}$ [11] more or less fits to a group of clusters with empty group 14 element cages linked by d block metal atoms (36 of the Ge atoms in $[Au_3Ge_{45}]^{9-}$ are part of $\{Ge_9\}$ cluster units), and thus retains molecular bonding characteristics, $[As@Ni_{12}@As_{20}]^{3-}$ [12] exhibits a unique highly symmetrical structure with a central As atom enclosed in an icosahedron of 12 Ni atoms that is surrounded by 20 As atoms in a pentagonal dodecahedral arrangement. This structural pattern of nested shells prompted the nicknames "onion-(skin-)like"[12] and "matryoshka nesting doll cluster".[13]

With the title compounds $A_{12}Cu_{12}Sn_{21}$, we herein present unique examples of polar intermetallic phases that feature such a discrete multiply endohedral intermetalloid cluster anion with a group 14 element: $[Sn@Cu_{12}@Sn_{20}]^{12-}$. Among the discrete intermetalloid cluster anions that appear in neat solid-state compounds, the new 33-atom Cu−Sn cluster is the first with a group 14 element, the first with a multiply endohedral onionskin-like structure, and currently the largest.

EXPERIMENTAL SECTION

Exploratory syntheses in the Na−Cu−Sn and K−Cu−Sn systems lead to $Na_{12}Cu_{12}Sn_{21}$ and $K_{12}Cu_{12}Sn_{21}$. Both compounds were structurally characterized by single-crystal XRD studies. Powder XRD data show that attempts to synthesize analogous compounds with the other alkali metals were successful for Rb and Cs.

Synthesis. *General Procedures.* All materials were handled in Ar atmosphere using an Ar-filled glovebox and other standard inert gas techniques. Na and K were purified by liquating, and Cu wire (99.9%, ChemPur), Cu powder (99.9%, Alpha Aesar), and Sn granules (99.999% ChemPur) were used as received. For the preparation of Cu−Sn alloys, Cu wire was melted together with Sn granula in an arc furnace installed in a glovebox, and the reguli were turned upside down and melted three times to ensure homogenization. To apply defined temperature programs the samples were sealed in Nb or Ta ampules, the ampules were placed in quartz tubes, which were evacuated, sealed, and inserted in vertical resistance tube furnaces.

Initial Syntheses of $A_{12}Cu_{12}Sn_{21}$ (A = Na, K). $Na_{12}Cu_{12}Sn_{21}$ was obtained as one of the products of a direct reaction of the elements in ratio Na:Cu:Sn = 1.00:1.00:3.00. For this 0.052 g of Na, 0.144 g of Cu powder, and 0.805 g of Sn were sealed in a Ta ampule. The temperature program applied consisted of three steps: heating to 850 °C at a rate of 2 K min^{-1}, holding at this temperature for 24 h, and cooling to room temperature at a rate of 0.1 K min^{-1}. The air-sensitive product was a dark gray/silver crystalline powder. Powder XRD analysis of the product (see Supporting Information, Figure S-1) showed the presence of the phase later established to be $Na_{12}Cu_{12}Sn_{21}$, together with several other phases, including the binary compounds $NaSn_5$ and Na_5Sn_{13}, as well as Cu and β-Sn, and at least one other, yet unreported phase. The latter was preliminarily characterized as a new ternary Na−Cu−Sn phase with the approximate composition $Na_{12-x}Cu_{20}Sn_{20+y}$ containing linear Cu−Sn nano rods.[14]

$K_{12}Cu_{12}Sn_{21}$ was isolated from the product of a reaction of K with a Cu−Sn phase that had been prepared by arc-melting elemental Cu and Sn in ratio Cu:Sn = 1.00:2.78. For this 0.162 g of Cu wire and 0.838 g of Sn were arc melted, and 0.890 g of the prepared Cu−Sn phase together with 0.110 g K were sealed in a Nb ampule. So the overall K:Cu:Sn ratio was 1.25:1.00:2.78. The sample was heated to 450 °C at a rate of 2 K min^{-1}, held at this temperature for 70 h, and then quenched to room temperature. The air-sensitive product was a gray/black powder containing lustrous black/silver crystals (with sizes up to approximately 0.5 mm) that could be separated readily from the powdery fraction. The powder XRD pattern of the product (see Supporting Information, Figure S-2) showed the reflections of the phase later identified as $K_{12}Cu_{12}Sn_{21}$ and the presence of Cu and at least one additional phase that could not yet be identified (indicated by three strong unindexed reflections in the range 2θ = 10.8−14.0°).

Syntheses with Stoichiometric Amounts A:Cu:Sn = 12:12:21 (A = Na, K, Rb, Cs). Reactions aimed at the synthesis of $A_{12}Cu_{12}Sn_{21}$ (A = Na, K, Rb, Cs) phases were subsequently carried out using stoichiometric amounts of Cu−Sn alloys (prepared by arc-melting Cu and Sn in ratio Cu:Sn = 12:21) and alkali metals, and employing reaction conditions as for the initial synthesis of $K_{12}Cu_{12}Sn_{21}$ (but with an increased isothermal dwelling time of 120 h). These reactions yielded the target compounds as main products (but not pure phase) in case of A = K, Rb, and Cs. $Na_{12}Cu_{12}Sn_{21}$ was only obtained as a minor byproduct.

Single-Crystal X-ray Diffraction and Crystal Structure Determination. Suitable single crystals of $Na_{12}Cu_{12}Sn_{21}$ and $K_{12}Cu_{12}Sn_{21}$ were selected in an Ar-filled glovebox equipped with a microscope. The block-shaped lustrous black/silver crystals were mounted on glass fibers that were fixed and sealed in glass capillaries. Single-crystal XRD data were collected at 20 °C with a STOE IPDS 2T imaging plate diffractometer using Mo K_α radiation (λ = 0.71073 Å, graphite monochromator, rotating anode source). For $Na_{12}Cu_{12}Sn_{21}$, a total of 540 frames were collected in three ω scans (ω = 0−180° with φ = 0°, 50°, and 75°) with an exposure time of 2 min and an ω increment of 1° per frame. For $K_{12}Cu_{12}Sn_{21}$, a total of 225 frames were collected in two ω scans (ω = 0−180° with φ = 0°, and ω = 0−45° with φ = 70°) with an exposure time of 2 min and an ω increment of 1° per frame.

The STOE X-AREA software[15] was used for data processing. Numerical absorption corrections were applied with X-RED[16]/X-SHAPE.[17] XPREP[18] was used for space group determination and data merging (identical indices only), and the programs XS[19,20] and XL[20,21] were used for structure solution (direct methods) and structure refinement (full-matrix least-squares on F_o^2), respectively. The structures were solved in space group $Pn\bar{3}m$ (No. 224).

The structure refinement for the K−Cu−Sn phase clearly showed that one K site, K4 (on 6d), is only partially occupied, while all other sites are fully occupied. (Free refinement of the occupancy parameters for the four K sites led to values of 1.00(1) for K1, 1.00(2) for K2, 0.99(2) for K3, and 0.67(2) for K4.) The final refined value for the site occupancy factor for K4 was 0.67(2), in perfect agreement with the value of 2/3 that results in a composition of K:Cu:Sn = 12:12:21. (Full occupancy of all alkali metal sites would lead to a composition of A:Cu:Sn = 12.5:12:21.) For the isotypic Na−Cu−Sn phase, free refinement of the occupancy factors for the four Na sites led to values of 0.99(2) for Na1, 0.99(3) for

Table 1. Selected Crystallographic, Data Collection, and Refinement Data for $A_{12}Cu_{12}Sn_{21}$ (A = Na, K)

formula	$Na_{12}Cu_{12}Sn_{21}$[a]	$K_{12}Cu_{12}Sn_{21}$[a]
formula weight, M/g mol^{-1}	3530.85	3724.17
space group	$Pn\bar{3}m$ (No. 224)	$Pn\bar{3}m$ (No. 224)
Z	4	4
unit cell parameter, a/Å	16.6253(3)	17.6100(5)
unit cell volume, V/Å^3	4595.2(1)	5461.1(3)
calculated density, ρ_{calc}/g cm^{-3}	5.104	4.530
absorption coefficient (Mo K_α), μ/mm^{-1}	16.701	14.874
F(000)	6120	6504
crystal color, shape	black/silver, block	black/silver, block
max. crystal dimensions/mm	0.15 × 0.10 × 0.10	0.14 × 0.16 × 0.12
temperature, T/K	293(2)	293(2)
wavelength (Mo K_α), λ/Å	0.71073	0.71073
diffractometer	STOE IPDS 2T (imaging plate)	STOE IPDS 2T (imaging plate)
θ range	3.68−26.83°	4.77−28.25°
limiting indices	$-21 \le h \le 21$; $-21 \le k \le 21$; $-21 \le l \le 21$	$-23 \le h \le 23$; $-23 \le k \le 23$; $-23 \le l \le 23$
reflections/unique	34 966/945	40 641/1285
completeness	98.7%	99.2%
R_σ, R_{int}	0.0097/0.0411	0.0143/0.0668
refinement method	full-matrix least-squares on F^2	full-matrix least-squares on F^2
data/restraints/parameters	945/0/50	1285/0/50
extinction		0.00030(2)
residual map/e Å^{-3}	+1.015 and −1.877	+1.362 and −1.440
GOF on F^2	1.643	1.519
R_1, wR_2 ($I > 2\sigma(I)$)	0.0354/0.0716	0.0400/0.0613
R_1, wR_2 (all data)	0.0356/0.0716	0.0417/0.0618

[a] See the Experimental Section for details on the refinement with partially occupied A sites.

Na2, 0.91(4) for Na3, and 0.96(4) for Na4, resulting in an overall composition of Na:Cu:Sn = 12.2(2):12:21, which is also in agreement with the formula $A_{12}Cu_{12}Sn_{21}$ (that is well within the 3σ limit). In the final refinement steps, full occupancy was assumed for Na1 and Na2, and the occupancy parameters for Na3 (on 8e) and Na4 (on 6d) were refined freely. The final refined values were 0.91(4) for Na3 and 0.96(4) for Na4.

Selected crystallographic data and refinement details are given in Table 1. Atomic coordinates, given in the Supporting Information (Table S-1), were standardized with the program STRUCTURE TIDY[22] implemented in PLATON.[23]

Powder X-ray Diffraction. For powder XRD analysis, samples of the reaction products were finely ground, diluted with diamond powder, and sealed in glass capillaries in an Ar-filled glovebox. Powder XRD data were collected with a STOE STADI P powder diffractometer equipped with a curved imaging plate and a linear position sensitive detector (IP-PSD, and L-PSD) using Cu $K_{\alpha1}$ radiation (λ = 1.54060 Å, curved Ge(111) monochromator).

EDX Measurement. An EDX analysis of a single crystal of $K_{12}Cu_{12}Sn_{21}$ (unit cell determined by single-crystal XRD previous to EDX analysis) was carried out using a JEOL 5900LV scanning electron microscope system. The analysis showed the presence of K, Cu, and Sn, and the absence of other elements heavier than Na.

Electronic Structure Calculations. Computational studies on the discrete $[Sn@Cu_{12}@Sn_{20}]^{12-}$ cluster were carried out using the Gaussian 09 package of programs (revision B.01).[24] In all calculations, either a background charge distribution made up of positive point charges was included or a continuous solvation model was used to compensate for the high negative charge of the cluster. All basis sets and the small core effective core potential for Sn were obtained from the EMSL Basis Set Exchange Library.[25,26] GAUSSVIEW[27] was used to visualize molecular orbitals.

For a single point calculation, the atomic positions deduced from a single-crystal XRD structure analysis of $K_{12}Cu_{12}Sn_{21}$ were used for the Cu and Sn atoms of the $[Sn@Cu_{12}@Sn_{20}]^{12-}$ cluster, and point charges of +1/3 each were placed at the positions of 36 K sites next to the cluster. This scheme was chosen because a comparison is made between the results of this Gaussian 09 calculation for the cluster anion and the results of the TB-LMTO-ASA calculations for the solid-state compound $K_{12}Cu_{12}Sn_{21}$. The B3LYP hybrid functional[28,29] was used with Def2-TZVP basis sets[30] for Cu and Sn and a small core effective core potential for Sn (ECP-28).[31] (This is referred to as B3LYP/(PP-)Def2-TZVP.) An analysis of the atomic contributions to molecular orbitals to support the inspection of MO plots was obtained with Gaussian 09. Natural charges were calculated using Version 3.1 of the NBO program[32] as implemented in Gaussian 09.

Structure optimizations for the $[Sn@Cu_{12}@Sn_{20}]^{12-}$ cluster were carried out starting with the experimentally observed structure (single-crystal XRD data for $K_{12}Cu_{12}Sn_{21}$). No restrictions in symmetry were applied. The optimized structure specified in the Supporting Information (Table S-5) was obtained using the B3LYP hybrid functional with Def2-SVP basis sets[30] for Cu and Sn and ECP-28 for Sn.[31] (This is referred to as B3LYP/(PP-)Def2-SVP.) The CPCM polarizable conductor calculation model[33,34] was employed with the solvent data for *N*,*N*-dimethylformamide (ε = 37.129), which is a solvent used in solution-based Zintl anion cluster chemistry. Default convergence criteria were used for the optimization with Gaussian 09. Formally, the high symmetry (D_{3d}) of the starting model was not retained during the optimization steps, but the optimized structure shows almost perfect icosahedral symmetry. The differences between interatomic distances that must be equal for an I_h symmetric structure are ≤0.012 Å (Table 2). Frequency calculations attest that the optimized structure corresponds to a minimum on the potential energy surface.

Table 2. Sn−Sn, Cu−Sn, and Cu−Cu Distances in $A_{12}Cu_{12}Sn_{21}$ (A = Na, K), and Calculated Interatomic Distances for $[Sn@Cu_{12}@Sn_{20}]^{12-}$

intracluster Sn−Sn, Cu−Sn, and Cu−Cu distances/Å					
	atoms	mult.[a]	$Na_{12}Cu_{12}Sn_{21}$	$K_{12}Cu_{12}Sn_{21}$	calculated[c]
{Sn@Cu_{12}@**Sn_{20}**}	Sn3−Sn2	6×	3.133(1)	3.133(1)	3.181−3.193
	Sn1−Sn1	6×	3.126(1)	3.123(1)	
	Sn1−Sn1	6×	3.096(1)	3.078(1)	
	Sn1−Sn2	12×	3.083(1)	3.076(1)	
{Sn@**Cu_{12}**@**Sn_{20}**}	Sn2−Cu2	12×	2.796(1)	2.781(1)	2.847−2.855
	Sn1−Cu1	12×	2.772(1)	2.765(1)	
	Sn1−Cu2	12×	2.764(1)	2.765(1)	
	Sn1−Cu1	12×	2.767(1)	2.759(1)	
	Sn2−Cu1	6×	2.748(2)	2.730(1)	
	Sn3−Cu2	6×	2.718(2)	2.734(1)	
{**Sn@Cu_{12}**@Sn_{20}}	Sn4−Cu1	6×	2.631(2)	2.628(1)	2.665−2.666
	Sn4−Cu2	6×	2.631(1)	2.622(1)	
{Sn@**Cu_{12}**@Sn_{20}}	Cu2−Cu2	6×	2.792(3)	2.780(2)	2.800−2.805
	Cu2−Cu1	12×	2.768(2)	2.761(1)	
	Cu1−Cu1	6×	2.762(2)	2.758(1)	
	Cu2−Cu1	6×	2.742(2)	2.738(2)	
intercluster Sn−Sn distances/Å					
	atoms	mult.[b]	$Na_{12}Cu_{12}Sn_{21}$	$K_{12}Cu_{12}Sn_{21}$	
cf. Figure 4d	Sn3−Sn3	1×	4.788(2)	5.454(2)	
	Sn2−Sn2	2×	4.814(1)	5.546(1)	
	Sn1−Sn1	2×	5.001(1)	5.718(1)	
cf. Figure 4c	Sn1−Sn1	2×	4.001(1)	4.644(1)	

[a] Multiplicity of interatomic distance within one {Sn@Cu_{12}@Sn_{20}} cluster. [b] Multiplicity of interatomic distance between two {Sn@Cu_{12}@Sn_{20}} clusters. [c] Structure optimization for $[Sn@Cu_{12}@Sn_{20}]^{12-}$ with B3LYP/(PP-)Def2-SVP and CPCM; default convergence criteria and no restrictions in symmetry applied.

To analyze the electronic structure of the $A_{12}Cu_{12}Sn_{21}$ (A = Na, K) solid-state phases, DFT calculations were carried out with the Stuttgart TB-LMTO-ASA program,[35] employing the tight-binding (TB) version of the linear muffin-tin orbital (LMTO) method in the atomic sphere approximation (ASA). The Barth−Hedin local exchange correlation potential[36] was used. Radii of the atomic spheres and interstitial empty spheres were determined by the procedures implemented in the TB-LMTO-ASA programs. The *k*-space integration was performed by the tetrahedron method.[37] 35 irreducible *k* points were used. Sn 5s/5p/(5d)/(4f), Cu 4s/4p/3d, and Na 3s/(3p)/(3d) or K 4s/(4p)/(3d) states were included in the calculations (down-folded in parentheses).

The partial occupancy of alkali metal sites cannot be treated computationally; thus the calculations were carried out for $A_{12.5}Cu_{12}Sn_{21}$ ($A_{50}Cu_{48}Sn_{84}$), assuming full occupancy of all positions. Within the rigid band approximation, the DOS calculated for $A_{12.5}Cu_{12}Sn_{21}$ reveals a band gap for both compositions $Na_{12}Cu_{12}Sn_{21}$ and $K_{12}Cu_{12}Sn_{21}$.

RESULTS

Crystal Structure. The isotypic compounds $Na_{12}Cu_{12}Sn_{21}$ and $K_{12}Cu_{12}Sn_{21}$ crystallize in the cubic space group $Pn\bar{3}m$ (No. 224). The structures feature discrete {Sn@Cu_{12}@Sn_{20}} cluster units, which are separated from each other by the alkali metal atoms. Thus, the formulas $A_{12}Cu_{12}Sn_{21}$ (A = Na, K) are used rather than $A_4Cu_4Sn_7$. The Cu−Sn clusters adopt a face centered cubic (fcc) arrangement (Figure 1), occupying the vertices and face centers of the cubic unit cell, albeit in different orientations. With increasing size of the alkali metal atoms, the lattice constant *a* increases considerably from *a* = 16.6253(3) Å for $Na_{12}Cu_{12}Sn_{21}$ to *a* = 17.6100(5) Å for $K_{12}Cu_{12}Sn_{21}$, and the distances between the clusters vary accordingly (Table 2).

The 33-atom {Sn@Cu_{12}@Sn_{20}} cluster shows an onionskin-type structure with a central Sn atom surrounded by a {Cu_{12}} icosahedron and a {Sn_{20}} pentagonal dodecahedron forming the outer shell (Figure 2). The cluster is set up by atoms on six independent positions. The Sn4 atom (Wyckoff 4b) resides at the center of the {Cu_{12}} icosahedron (6 × Cu1 on 24k and 6 × Cu2 on 24k) that is surrounded by 20 Sn atoms (12 × Sn1 on 48l, 6 × Sn2 on 24k, and 2 × Sn3 on 8e) that cap the 20 faces of the {Cu_{12}} icosahedron, thereby forming an almost ideal {Sn_{20}} pentagonal dodecahedron. Thus, the {Cu_{12}} and {Sn_{20}} structural shells of the cluster are arranged according to the dual relationship of the icosahedron and the pentagonal dodecahedron, with the vertices of one polyhedron pointing to the centers of the faces of the other, and vice versa. The structure of the {Sn@Cu_{12}@Sn_{20}} clusters is crystallographically confined to D_{3d} point symmetry, one of the highest subgroups of I_h, which itself cannot be imposed by crystallographic conditions, and the clusters possess only one crystallographic $\bar{3}$ axis (Figure 2). However, the structure of the cluster shows only small deviations from perfect icosahedral point symmetry I_h, as it can be seen from

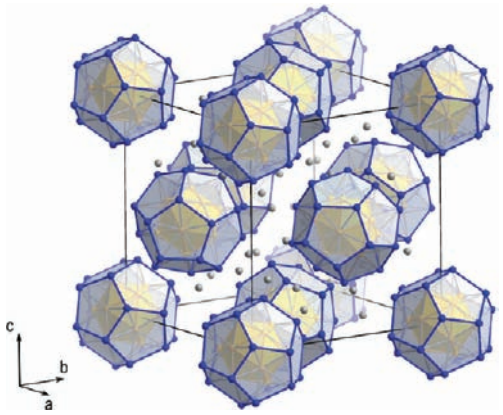

Figure 1. Representation of the unit cell of the $A_{12}Cu_{12}Sn_{21}$ phases. The $\{Sn@Cu_{12}@Sn_{20}\}$ clusters adopt a face centered cubic (fcc) arrangement. Sn atoms are represented with blue, Cu atoms with orange, and A atoms with gray color.

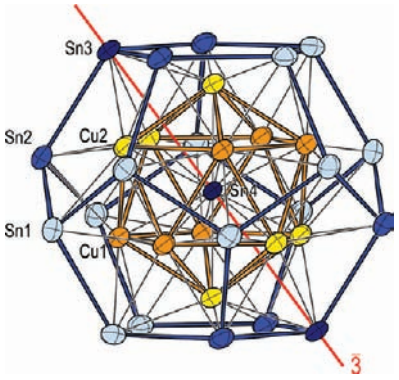

Figure 2. Representation of the $\{Sn@Cu_{12}@Sn_{20}\}$ cluster units in $A_{12}Cu_{12}Sn_{21}$. Sn atoms are represented with blue, and Cu atoms with orange color. Different color shades are used to distinguish the Wyckoff positions. The crystallographic 3-fold inversion axis $\bar{3}$ is drawn as a red line. Thermal ellipsoids are shown with 70% probability level for $K_{12}Cu_{12}Sn_{21}$.

a list of all intracluster first neighbor distances in $Na_{12}Cu_{12}Sn_{21}$ and $K_{12}Cu_{12}Sn_{21}$ (Table 2).

The Sn−Sn distances within the $\{Sn_{20}\}$ pentagonal dodecahedra range from 3.076(1) to 3.133(1) Å. Between the outer $\{Sn_{20}\}$ shells and the enclosed $\{Cu_{12}\}$ icosahedra, Cu−Sn distances of 2.718(2)−2.796(1) Å are found. Within the $\{Cu_{12}\}$ icosahedra, the Cu−Cu distances lie between 2.738(2) and 2.792(3) Å, and the Cu−Sn distances between the Cu atoms of the $\{Cu_{12}\}$ shells and the central Sn atoms range from 2.622(1) to 2.631(2) Å. The icosahedral theme dominates the coordination environment of the atoms of the cluster's inner structural shells (Sn4, Cu1, and Cu2). The central Sn4 atom has a full icosahedral coordination environment, the coordination number of the Cu1 and Cu2 atoms is 11 (1 × Sn4, 2 × Cu1, 3 × Cu2, 4 × Sn1, 1 × Sn2 for Cu1; 1 × Sn4, 3 × Cu1, 2 × Cu2, 2 × Sn1, 2 × Sn2, 1 × Sn3 for Cu2), and the associated coordination polyhedron is an incomplete icosahedron missing one vertex. Each of the Sn1, Sn2, and Sn3 atoms of the outer $\{Sn_{20}\}$ structural shell has coordination number six within the cluster, in view of three other Sn atoms as next neighbors in the

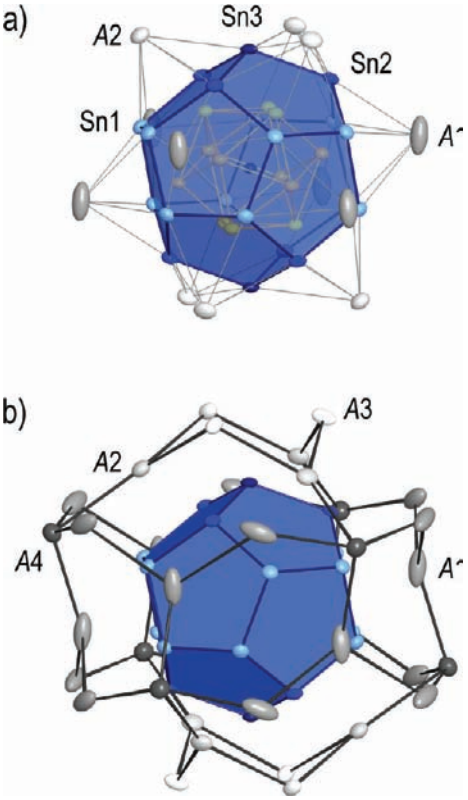

Figure 3. Coordination of the $\{Sn@Cu_{12}@Sn_{20}\}$ clusters with alkali metal atoms A in $A_{12}Cu_{12}Sn_{21}$. (a) $\{Sn@Cu_{12}@Sn_{20}\}$ cluster with 12 A atoms capping the faces of the $\{Sn_{20}\}$ pentagonal dodecahedron. (b) $\{Sn_{20}\}$ pentagonal dodecahedron with the 36 next nearest A sites. Sn atoms are represented with blue, Cu atoms with orange, and A atoms with gray color. Different color shades are used to differentiate the Wyckoff positions. Thermal ellipsoids are shown with 70% probability level for $K_{12}Cu_{12}Sn_{21}$.

$\{Sn_{20}\}$ pentagonal dodecahedron and, by capping a face of the $\{Cu_{12}\}$ icosahedron, contact to three Cu atoms.

Each $\{Sn@Cu_{12}@Sn_{20}\}$ cluster is surrounded by 36 alkali metal sites (18 × A1, 6 × A2, 6 × A3, and 6 × A4), and 12 of them (6 × A1 and 6 × A2) cap the 12 pentagonal faces of the cluster's $\{Sn_{20}\}$ shell (Figure 3a), thereby completing the coordination polyhedra of the Cu1 and Cu2 atoms to icosahedra, and joining in the pseudo 5-fold symmetry exhibited by the Cu−Sn clusters. This (pseudo) symmetry is lost, however, in the coordination of the clusters by the other A atoms. The whole structural motif, which is configured by the 36 A sites around a $\{Sn@Cu_{12}@Sn_{20}\}$ cluster (Figure 3b), is not related to a regular polyhedron. The shortest A−Sn distances are 3.141(6)−3.681(7) Å for A = Na, and 3.471(2)−3.966(3) Å for A = K.

The Cu−Sn distances in the $\{Sn@Cu_{12}@Sn_{20}\}$ clusters (2.622(1)−2.796(1) Å) match those in binary Cu−Sn bronzes (e.g., 2.631−2.860 Å in η'-bronze, the low temperature modification of the Sn richest binary Cu−Sn phase Cu_6Sn_5[38]), as well as those in the Cu−Sn structure parts of certain polar intermetallic phases, for example, 2.585(1)−2.869(1) Å in $Ca_3Cu_8Sn_4$ and $CaCu_9Sn_4$,[39] which show structural motifs of face sharing and/or directly interconnected (distorted) icosahedra build of Cu and Sn atoms with Cu atoms in the center, and also those in the soluble anionic Cu−Sn cluster $[Cu@Sn_9]^{3-}$[40] (2.611(7)−2.700(7) Å).

As for the Cu−Cu distances, those in the $\{Sn@Cu_{12}@Sn_{20}\}$ clusters (2.738(2)−2.792(3) Å) are significantly longer than those in elemental Cu (2.555 Å), at the upper limit of those observed in binary Cu−Sn phases (e.g., 2.537−2.720 Å in η'-Cu_6Sn_5), and within the range of those found for the above-mentioned Ca−Cu−Sn phases[39] (2.532(4)−2.956(2) Å).

The Sn−Sn distances within the $\{Sn_{20}\}$ structural shell of the $\{Sn@Cu_{12}@Sn_{20}\}$ clusters (3.076(1)−3.133(1) Å) compare well with those of metallic β-Sn (3.016 and 3.175 Å) and those of the smaller intermetalloid clusters $[Cu@Sn_9]^{3-}$ [40] with a $\{Sn_9\}$ tricapped trigonal prism (3.0236(5)−3.1556(5) Å, not regarding the longer prism heights) and $[Ir@Sn_{12}]^{3-}$ [41] with a $\{Sn_{12}\}$ icosahedron (3.0250(8)−3.1004(9) Å). They are slightly longer than those found for empty homoatomic Zintl cluster anions of Sn, which also show Sn−Sn distances < 3.0 Å (e.g., 2.949(1) Å for tetrahedral $[Sn_4]^{4-}$ in KSn,[42,43] and d(Sn−Sn) ≥ 2.9264(9) Å for monocapped square antiprismatic $[Sn_9]^{4-}$ in K_4Sn_9[44]). These smaller deltahedral Sn cages mostly follow Wade's Rules for the electron count of clusters, and delocalized bonding between the Sn atoms is assumed for them.

In other Zintl phases and related stannides, Sn−Sn distances in the range of typical Sn−Sn covalent bond length of ∼2.8 Å (cf. 2.810 Å in α-Sn), or slightly elongated Sn−Sn distances up to ∼2.9 Å are found. Examples include K_8Sn_{44},[45] $K_{6+x}Sn_{25}$,[46,47] and $A_3Na_{10}Sn_{23}$ (A = K, Rb, Cs)[48] with extended Sn substructures featuring pentagonal dodecahedral structure motifs, as well as $Ba_{16}Na_{204}Sn_{310}$[49] and $AeNa_{10}Sn_{12}$ (Ae = Ca, Sr)[50] with discrete $\{Ba_4@Sn_{56}\}$ or $\{Ae@Sn_{12}\}$ clusters, respectively. As for the structures of these Sn clusters, the $\{Sn_{56}\}$ cage is described as four fused pentagonal dodecahedra, and the $\{Sn_{12}\}$ cage as a truncated tetrahedron.

The longer Sn−Sn distances in $\{Sn@Cu_{12}@Sn_{20}\}$ clearly suggest that the interactions between the Sn atoms in this Cu−Sn cluster are more delocalized in character, as is expected for an intermetalloid species.

Despite some details concerning their orientation, the $\{Sn@Cu_{12}@Sn_{20}\}$ clusters are arranged in analogy to a face centered cubic atom packing, and each cluster has 12 neighbors in the $A_{12}Cu_{12}Sn_{21}$ structure. The mutual orientation of the clusters and the resulting different intercluster Sn−Sn distances can be shown focusing on a cuboctahedral subunit of 13 (1 + 12) clusters (Figure 4). The shortest intercluster Sn−Sn distances between the central cluster and its neighbors occur between Sn1−Sn1 edges of both the central cluster and its six neighbors in its equatorial plane perpendicular to its 3-fold axis (labeled as B in Figure 4); these are 4.001(1) Å for $Na_{12}Cu_{12}Sn_{21}$ and 4.644(1) Å for $K_{12}Cu_{12}Sn_{21}$ (Figure 4c, Table 2). In the two tetrahedral subunits of the cuboctahedral cluster array that are formed by the central cluster and three clusters each of layer A and C (Figure 4), each of the four clusters faces its three neighbors with the three pentagonal faces meeting at one of its Sn3 vertices (Figure 4d). The clusters' $\bar{3}$ axes point to the centers of the resulting supertetrahedra of clusters, and opposing pentagonal faces are (quasi) parallel, with associated intercluster Sn−Sn distances of 4.788(2) Å (Sn3−Sn3), 4.814(1) Å (Sn2−Sn2, 2×), and 5.001(1) Å (Sn1−Sn1, 2×) for $Na_{12}Cu_{12}Sn_{21}$ and 5.454(2) Å (Sn3−Sn3), 5.546(1) Å (Sn2−Sn2, 2×), and 5.718(1) Å (Sn1−Sn1, 2×) for $K_{12}Cu_{12}Sn_{21}$ (Figure 4d, Table 2).

The remarkably large changes in intercluster distances for $Na_{12}Cu_{12}Sn_{21}$ and $K_{12}Cu_{12}Sn_{21}$, and virtually identical interatomic distances within the cluster units in both phases (Table 2), further establish the clusters as discrete units and support the interpretation of the title phases as salt-like intermetallic compounds.

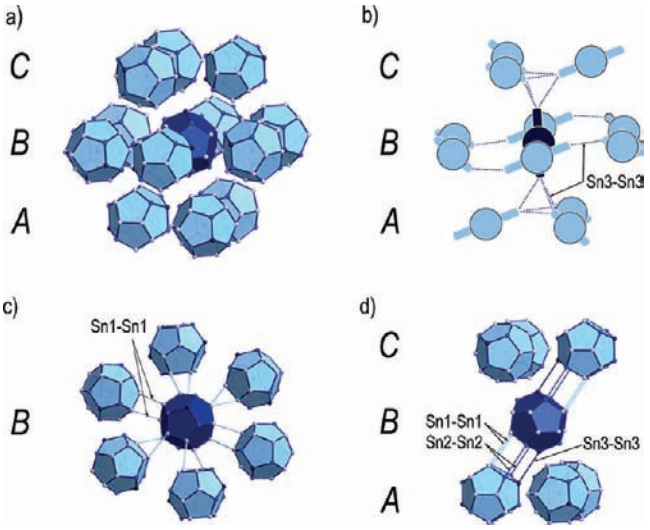

Figure 4. Packing of the (pseudo)dodecahedral $\{Sn@Cu_{12}@Sn_{20}\}$ clusters in $A_{12}Cu_{12}Sn_{21}$. Selected intercluster Sn−Sn distances are shown, while Cu atoms are omitted for clarity. (a) Representation of 12 $\{Sn@Cu_{12}@Sn_{20}\}$ clusters (light blue) around a central cluster (dark blue) in a cuboctahedral subunit of the face centered cubic arrangement. The ABC stacking sequence of hexagonal close packed layers is indicated, with the layers perpendicular to the central cluster's $\bar{3}$ axis. (b) Schematic representation of the unit shown in (a). Clusters are represented as spheres with sticks designating the clusters' $\bar{3}$ axes that run through the Sn3 atoms. (c) Section with the central cluster and its six neighbors in layer B. The representation is inclined with respect to the one in (a), and the $\bar{3}$ axis of the central cluster points out of the plane of projection. The shortest intercluster Sn−Sn distances are found between Sn1−Sn1 edges of both the central cluster and its six neighbors. (d) The central cluster and its six other neighbors with quasi parallel pentagonal faces. For clarity, only the associated intercluster Sn−Sn distances between the central cluster and two of its neighbors are shown.

Electronic Structure Calculations. Assuming a full charge separation between the alkali metal atoms and the Cu−Sn clusters in $A_{12}Cu_{12}Sn_{21}$ leads to a count of 12 A^+ cations per cluster unit, and thus the clusters may be regarded as discrete $[Sn@Cu_{12}@Sn_{20}]^{12-}$ anions. Hybrid DFT calculations have been performed for $[Sn@Cu_{12}@Sn_{20}]^{12-}$ to analyze the steric configuration and the electronic structure of the intermetalloid cluster.

Structure optimizations confirm the highly symmetric structure of the discrete $[Sn@Cu_{12}@Sn_{20}]^{12-}$ cluster. Using B3LYP/(PP-)Def2-SVP (with the CPCM solvation model for charge compensation), a structure that shows virtually no distortion from I_h symmetry (interatomic distances are quoted in Table 2, atomic coordinates are given in the Supporting Information, Table S-5) was reached in the optimization, and the frequency calculation verified that this corresponds to a ground state. The calculated interatomic distances are in good agreement with those determined experimentally by single-crystal XRD structure analysis (Table 2). Default convergence criteria were used for the optimization, and the calculated Sn−Sn distance within the $\{Sn_{20}\}$ pentagonal dodecahedron is 3.18−3.19 Å, the optimized Cu−Cu distance within the $\{Cu_{12}\}$ icosahedron is 2.80−2.81 Å, and Cu−Sn distances of 2.85−2.86 and 2.66−2.67 Å were calculated for the Cu−Sn next neighbors involving Sn atoms of the $\{Sn_{20}\}$ pentagonal dodecahedron and the central Sn atom, respectively.

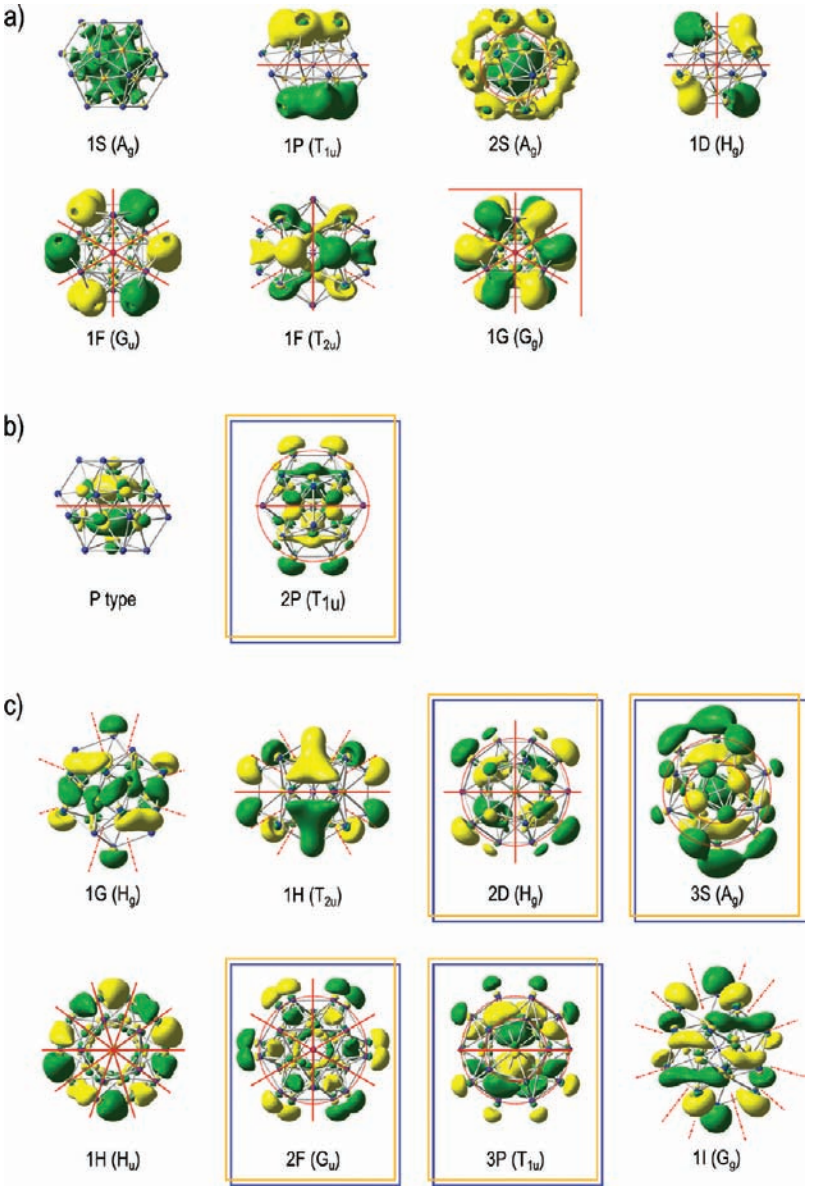

Figure 5. Molecular orbitals (MOs) of the $[Sn@Cu_{12}@Sn_{20}]^{12-}$ cluster anion. (a) MOs with mainly Sn s type atomic contributions (Sn s block). (b) P type MOs with Sn p type contributions from the central Sn atom. (c) MOs dominated by Sn p type contributions from the Sn atoms of the $\{Sn_{20}\}$ structural shell (Sn p block). (Selected MO plots for Cu d block MOs are given in the Supporting Information, Figure S-4.) Red circles indicate radial nodal surfaces, red solid lines show angular nodes perpendicular or parallel to the plane of projection, and red dotted lines symbolize conical angular nodes.

A single point calculation with B3LYP/(PP-)Def2-TZVP using atomic coordinates deduced from single-crystal XRD data (with point charges placed at the positions of the alkali metal atoms to compensate for the high negative charge of the cluster) showed a HOMO−LUMO gap of 1.34 eV.

A natural population analysis indicates that besides Sn s and p, and Cu d states, also Cu 4s and 4p states are populated to a notable extent, and that the negative charge is distributed rather evenly throughout the whole cluster. The calculated natural charges are −0.33 to −0.52 for the $\{Sn_{20}\}$ Sn atoms, −0.22 to −0.26 for the $\{Cu_{12}\}$ Cu atoms, and −0.17 for the central Sn atom.

An inspection of the MO plots for the $[Sn@Cu_{12}@Sn_{20}]^{12-}$ clusters shows that these can be described according to a scheme that has also been used in MO analyses for a number of p block element cage cluster ions and their (singly) endohedral derivatives.[4] The representations of cluster MOs are found to resemble those of atomic orbitals, and labels S, P, D, F, G, H, I, etc., are used for cluster MOs with 0, 1, 2, 3, 4, 5, 6, etc., angular nodes, respectively; labels 1, 2, 3, etc., are used for MOs with 0, 1, 2, etc., radial nodal surfaces, respectively. The cage cluster MOs are based on s and p type atomic contributions of the p block element atoms. For cage clusters with a single endohedral d block element atom in the cluster center, there is an additional block of MOs based on the atomic d orbitals of the central atom, and the MOs of such filled clusters show mixing of suitable cage- and guest-based contributions. The main stabilizing effect is attributed to interactions involving s and p type contributions of the central atom.

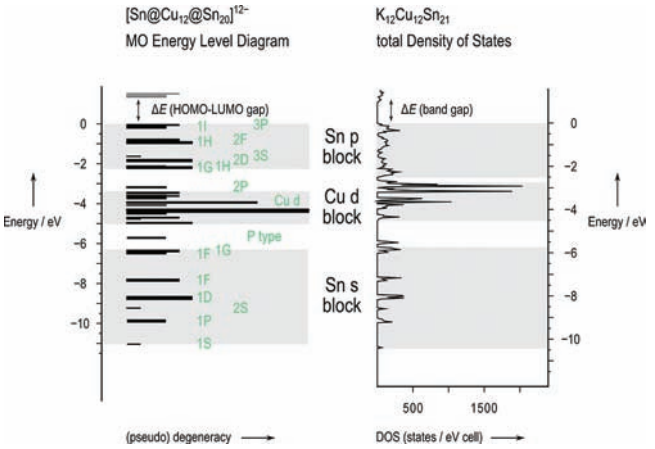

Figure 6. MO energy level diagram for the $[Sn@Cu_{12}@Sn_{20}]^{12-}$ cluster anion (single point calculation with B3LYP/(PP-)Def2-TZVP and point charges for charge balance), and total density of states for $K_{12}Cu_{12}Sn_{21}$ (TB-LMTO-ASA calculation). Both the HOMO energy and the Fermi level were set to 0 eV.

For $[Sn@Cu_{12}@Sn_{20}]^{12-}$, the allocation of the nodes is best practiced following the s and p type contributions of the Sn atoms. For the members of the second series of cluster MOs with $\{Sn_{20}\}$ Sn p-radial contributions (corresponding to Sn atomic p orbitals oriented radially), the $\{Sn_{20}\}$ structural shell defines the radial nodal surface, and the third series (3S, 3P) shows two radial nodal surfaces. Although the following MO analysis is based on the results of the single point calculation that was performed with the experimentally obtained structural data (D_{3d} symmetry) for $[Sn@Cu_{12}@Sn_{20}]^{12-}$, for clarity, the labels for the irreducible representations of the I_h point group are used in the discussion. In I_h point group symmetry, S type orbitals show a_g symmetry, P type orbitals transform as t_{1u}, D type orbitals as h_g, F type orbitals split into two sets of t_{2u} and g_u symmetry, G type orbitals into two sets transforming as g_g and h_g, H type oribtals split into three sets of t_{1u}, t_{2u}, and h_u symmetry, and I type orbitals transform as a_g, t_{1g}, g_g, and h_g.

The 21 lowest lying MOs of the $[Sn@Cu_{12}@Sn_{20}]^{12-}$ cluster may be characterized as Sn s block; that is, atomic contributions of Sn s type dominate their appearance (Figure 5a). They can be labeled 1S (A_g), 1P (T_{1u}), 2S (A_g), 1D (H_g), 1F (G_u), 1F (T_{2u}), and 1G (G_g). Both the central Sn atom and the $\{Sn_{20}\}$ Sn atoms contribute to the 1S (A_g) and 2S (A_g) cluster MOs. The MOs classified as 1F (T_{2u}) and 1G (G_g) show considerable in-phase mixing with Cu d type contributions, and for the 2S (A_g) MO also Cu d type admixing is found. The population analysis further shows contributions of Cu s type to 1S, 1P, 1D, 1F (T_{2u}) and of Cu p type to 1P, 2S, 1D, 1F (G_u). Except for the 1F (T_{2u}) and 1G (G_g) MO sets, which are almost equal in energy, the MO sets of the Sn s block are energetically well separated from each other (see Figure 6 and Supporting Information, Table S-6). Next in energy is a set of P type MOs (labeled as "P type" in Figure 5b) showing in-phase mixing of contributions of Sn p type by the central Sn atom and Cu s, p, and d type (according to the population analysis). This MO set is energetically well separated both from the underlying Sn s block MOs and from the following block of 57 MOs that is dominated by Cu d type contributions (MO plots for selected Cu d block MOs are shown in the Supporting Information, Figure S-4). As the 1F (T_{2u}) and 1G (G_g) $\{Sn_{20}\}$ Sn s block MO sets showed in-phase mixing with Cu d type contributions, antibonding $\{Sn_{20}\}$ Sn-based cage F and G type admixing is found for two of the MO sets of this Cu d block. The population analysis also indicates some Sn s and p type admixing by the central Sn atom to suitable MOs of this Cu d block (together with minor $\{Sn_{20}\}$ Sn-based and Cu s type contributions), and some Cu s type admixing is found to energetically lower lying Cu d block MOs. Only a minor gap in energy is found between these Cu d block MOs and a set of P type MOs that may be classified as 2P cluster MOs (labeled as "2P" in Figure 5b). Sn p type contributions of both the central Sn atom and the $\{Sn_{20}\}$ Sn atoms (p-radial) as well as Cu s and d type admixing can be identified for these 2P MOs. A considerable gap in energy separates these 2P MOs from the following 30 highest occupied MOs that in the main may be classified as $\{Sn_{20}\}$ Sn p block (Figure 5c). The MOs are labeled 1G (H_g), 1H (T_{2u}), 2D (H_g), 3S (A_g), 1H (H_u), 2F (G_u), 3P (T_{1u}), 1I (G_g). The 1G, 1H, and 1I MOs, with no radial and a high number of angular nodes, show a high share of $\{Sn_{20}\}$ Sn p-tangential contributions and may be described as surface bonding in the main, although, except 1H (H_u), they also show some lone pair character. The population analysis indicates Cu s (and minor d) type contributions to 1G (H_g) and 1H (T_{2u}), and Cu d type admixing to 1I (G_g). For the 2D, 3S, 2F, and 3P MOs, the $\{Sn_{20}\}$ structural shell defines a radial node, and thus mostly $\{Sn_{20}\}$ Sn p-radial type contributions, which correspond to atomic Sn p orbitals pointing to the $\{Cu_{12}\}$ icosahedral surface, are found for these MOs. For the 2D and the 2F MOs, the population analysis indicates contributions of Cu p type (and admixing of Cu d type to 2F and to a minor extent Cu s type to 2D). Cu p-tangential contributions, corresponding to atomic Cu p orbitals oriented tangentially to the $\{Cu_{12}\}$ shell, show in-phase overlap with the $\{Sn_{20}\}$ Sn p-radial contributions. The 3S and 3P MOs show contributions from all three structural shells. For the 3S, these are of Sn s type by the central Sn atom, Cu s and d type, and $\{Sn_{20}\}$ Sn p-radial type. For the 3P MOs, the sequence of Sn p type contributions by the central Sn atom, Cu-based contributions, and $\{Sn_{20}\}$ Sn p-radial contributions, pervades the whole cluster.

The electron configuration of the $[Sn@Cu_{12}@Sn_{20}]^{12-}$ cluster may be summarized as $1S^2\ 1P^6\ 2S^2\ 1D^{10}\ 1F^8\ 1F^6\ 1G^8$ (P type MO)^6 ("pure" Cu d block)^{114} $2P^6\ 1G^{10}\ 1H^6\ 2D^{10}\ 3S^2\ 1H^{10}\ 2F^8\ 3P^6\ 1I^8$. Only the third series of cluster MOs shows a closed shell configuration ($3S^2\ 3P^6$); for the first series the occupation is $1S^2\ 1P^6\ 1D^{10}\ 1F^{14}\ 1G^{18}\ 1H^{16}\ 1I^8$ (both 1H and 1I open shell), and for the second series the occupation is $2S^2\ 2P^6\ 2D^{10}\ 2F^8$ (open F shell). The MO analysis shows several MOs comprising contributions of two or all three structural shells. Cu p (and some s) type participation is found for MOs that show important in-phase mixing involving such contributions from different structural shells, which supposedly plays a part for the stability of the cluster. These bonding interactions for $[Sn@Cu_{12}@Sn_{20}]^{12-}$ may be seen to parallel the Cu p (and s) type involvement in bonding interactions for $[Cu@Sn_9]^{3-}$.[40]

The conceptual treatment of $[Sn@Cu_{12}@Sn_{20}]^{12-}$ as a discrete cluster anion and the $A_{12}Cu_{12}Sn_{21}$ phases as salt-like in character is further supported by the existence of the isostructural and iso(valence)electronic anion $[As@Ni_{12}@As_{20}]^{3-}$ that was obtained from a reaction of soluble precursors and characterized in the salt $[Bu_4P]_3[As@Ni_{12}@As_{20}]\cdot 1.5en$[12] (Bu, butyl-; en, ethylendiamin). In an MO analysis for $[As@Ni_{12}@As_{20}]^{3-}$, based on extended Hückel calculations, atomic p type contributions from the d block metal atoms have been assigned an important role in bonding interactions, similar to what has been shown in the above MO analysis for $[Sn@Cu_{12}@Sn_{20}]^{12-}$.

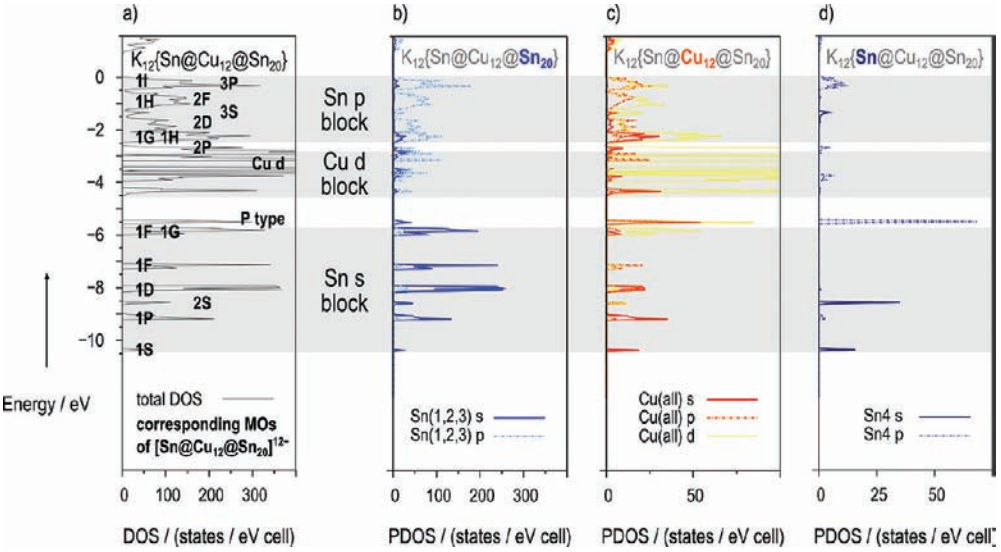

Figure 7. Total and partial density of states (DOS) curves for $K_{12}Cu_{12}Sn_{21}$. (a) Total DOS curve with DOS peaks marked with the labels for the corresponding molecular orbitals of $[Sn@Cu_{12}@Sn_{20}]^{12-}$ (cf. Figure 6). (b) Partial density of states (PDOS) curves for the Sn atoms of the $\{Sn_{20}\}$ pentagonal dodecahedra. (c) PDOS curves for the Cu atoms. (d) PDOS curves for the central Sn atoms of the $\{Sn@Cu_{12}@Sn_{20}\}$ clusters. The Fermi level for $K_{12}Cu_{12}Sn_{21}$ was set to 0 eV.

A leading thought in accounts on the electronic structure of $[As@Ni_{12}@As_{20}]^{3-}$, both in the original[12] a subsequent work,[13] is the partitioning of the cluster into subshells, entailing a focus on the "individual" electronic requirements of these subshells and their satisfaction. A major difficulty that comes along with the employed electron counting schemes concerns the As−As interactions in the $\{As_{20}\}$ shell: 60 electrons are located in two center two electron bonds for the 30 dodecahedral edges of the $\{As_{20}\}$ cage, albeit the As−As bonding is characterized as weak in view of rather long As−As distances and the results of LDI-TOF MS experiments. A detailed analysis of these discussions on the electronic structure of $[As@Ni_{12}@As_{20}]^{3-}$ is included in the Supporting Information (Text S-2). It has already been mentioned above that the Sn−Sn distances in $[Sn@Cu_{12}@Sn_{20}]^{12-}$ are also significantly longer than those in related structures with prevalent covalent two-center bonding.

To analyze the electronic structure of the $A_{12}Cu_{12}Sn_{21}$ (A = Na, K) solid-state phases, band structure calculations were carried out for $A_{12.5}Cu_{12}Sn_{21}$ ($A_{50}Cu_{48}Sn_{84}$) models, that is, with full occupancy of all A positions. Within the rigid band approximation, the calculated DOS reveals a band gap for $A_{12}Cu_{12}Sn_{21}$ ($A_{48}Cu_{48}Sn_{84}$) for both the Na and the K compounds. The calculated band gap increases with increasing size of the cations and thus increasing intercluster distances from 0.3 eV for $Na_{12}Cu_{12}Sn_{21}$ to 0.8 eV for $K_{12}Cu_{12}Sn_{21}$. Thus, the electronic structure resembles those of Zintl phases with homoatomic cluster anions, and the title compounds can be considered as salt-like phases. The calculated DOS curves (Figures 6 and 7 and Supporting Information, Figures S-5 and S-6) approve that the $A_{12}Cu_{12}Sn_{21}$ phases provide a textbook example for a molecular unit in a solid-state compound, very structured with gaps and pseudogaps reflecting the energetic ordering of the cluster MOs (Figure 6). As it can be seen from a comparison of the MO analysis given above and the partial DOS (PDOS) curves shown in Figure 7, not only is the general partitioning with a Sn s block, a Cu d block, and a Sn p block also revealed for the electronic structure of the solid-state phase, there is a clear correspondence between individual DOS peaks and sets of MOs (Figures 6 and 7a), and also the partial DOS contributions (Figure 7) are in good agreement with the atomic contributions found in the MO analysis for the $[Sn@Cu_{12}@Sn_{20}]^{12-}$ cluster. For example, the important Cu p type contributions to states in the Sn p block, or the Sn4 s type or p type contributions to 3S or 3P states, respectively, are also revealed by the PDOS analysis.

DISCUSSION

For Zintl phases comprised of an electropositive metal A (e.g., an alkali metal) and a more electronegative p block (semi)metal E, a complete electron transfer from A to E is assumed, and the phases are rationalized in terms of ionic interactions between the cationic and the anionic substructures. For the very classical Zintl phases, the anionic substructures abide to the $8 - N$ rule for covalent bonding. The concept has been extended, and homoatomic deltahedral cluster units in the anionic substructures of Zintl phases, such as the discrete $[Sn_9]^{4-}$ nido cluster anions in K_4Sn_9, are conveniently explained with the help of Wade's rules for cluster bonding.

Even though the title phases contain a considerable amount of transition metal, and the electronic structure of the intermetalloid $[Sn@Cu_{12}@Sn_{20}]^{12-}$ clusters cannot be rationalized by the rules that apply to the smaller p block element clusters, the results of the band structure calculations show that the $A_{12}Cu_{12}Sn_{21}$ phases may also be considered as salt-like compounds just like the Zintl phases.

The MO analysis for $[Sn@Cu_{12}@Sn_{20}]^{12-}$ shows that the cluster can be viewed as a whole, rather than focusing on a partitioning into different subshells with individual electronic requirements. The bonding within and between the cluster's structural shells is delocalized and best expressed as "intermetalloid cluster bonding".

The cubic packing of the intermetalloid Cu−Sn cluster anions in the title phases follows patterns known from other species with (pseudo)icosahedral symmetry.[51] The $C_{20}H_{20}$ dodecahedran molecules with pentagonal dodecahedral

structure adopt an fcc arrangement and crystallize in a cubic space group,[52,53] and so do the C_{60} fullerene molecules,[54−56] as well as the icosahedral $[B_{12}H_{12}]^{2-}$ borane cluster anions in the alkali metal compounds $A_2B_{12}H_{12}$ (A = K,[57] Cs[58]). An insightful analysis that also highlights the relationships between icosahedral and octahedral (cubic) symmetry of polyhedra has been given recently.[51]

The structure of the $\{Sn@Cu_{12}@Sn_{20}\}$ clusters, with a central atom surrounded by an icosahedral shell of 12 atoms enclosed in a 20-atom pentagonal dodecahedron, can be related to the core of the cluster aggregates in the $Mg_{32}(Al,Zn)_{49}$ structure type. Notably, ternary intermetallic phases with an alkali metal, a group 10 metal, and a group 14 element that adopt $Mg_{32}(Al,Zn)_{49}$ type structures have been reported in the systems Li−Cu−Si, and Na−Au−E with E = Si, Ge, and Sn.[59] However, this is merely a structural analogy. The $\{Sn@Cu_{12}@Sn_{20}\}$ clusters in the $A_{12}Cu_{12}Sn_{21}$ phases are discrete anionic intermetalloid clusters separated by alkali metal cations. For the compounds with $Mg_{32}(Al,Zn)_{49}$ type structures, the structural shells do not correspond to such a separation.

CONCLUSION

The synthesis of the ternary A−Cu−Sn phases $A_{12}Cu_{12}Sn_{21}$ (A = K, Rb, Cs) by reaction of a binary Cu−Sn alloy with an alkali metal parallels the formation of a binary Zintl phase from a more electronegative p block (semi)metal and an electropositive metal (e.g., an alkali metal). Also, just as homoatomic anionic clusters of p block (semi)metals, such as $[Sn_9]^{4-}$ in K_4Sn_9,[44] are seen as small charged element particles,[60] the $[Sn@Cu_{12}@Sn_{20}]^{12-}$ clusters in the $A_{12}Cu_{12}Sn_{21}$ phases can be regarded as small charged alloy particles or "bronze dots".

The (electronic) structure of the title compounds suggests a description by means of an extension of the salt-like description of (polar) intermetallics introduced by Eduard Zintl, even though concepts like the $8 - N$ rule or Wade's rules are not yet obvious for the description of the structure and bonding of the transition metal rich anionic substructure in the $A_{12}Cu_{12}Sn_{21}$ phases, the $[Sn@Cu_{12}@Sn_{20}]^{12-}$ cluster anions.

ASSOCIATED CONTENT

Supporting Information. Complete ref 23. Powder XRD patterns of the products of initial Syntheses of $A_{12}Cu_{12}Sn_{21}$ (A = Na, K). Tables of positional and thermal parameters, anisotropic displacement parameters, and important distances as well as X-ray crystallographic files in CIF format for $Na_{12}Cu_{12}Sn_{21}$ and $K_{12}Cu_{12}Sn_{21}$. A description of the alkali metal substructure in the $A_{12}Cu_{12}Sn_{21}$ phases. Table of atomic coordinates for the optimized structure of the $[Sn@Cu_{12}@Sn_{20}]^{12-}$ cluster, table of MO energy values for the single point calculation, and a figure of MO plots for selected Cu d block MOs. Discussion of some accounts given on the electronic structure of $[As@Ni_{12}@As_{20}]^{3-}$. Figures with additional (P)DOS curves for $K_{12}Cu_{12}Sn_{21}$ and (P)DOS curves for $Na_{12}Cu_{12}Sn_{21}$. This material is available free of charge via the Internet at http://pubs.acs.org.

AUTHOR INFORMATION

Corresponding Author
thomas.faessler@lrz.tum.de

ACKNOWLEDGMENT

We thank F. Krause, R. Brimioulle, and J. Kraus who carried out experimental work on the synthesis of the title compounds. S.S. would also like to thank the Studienstiftung des Deutschen Volkes for a Ph.D. fellowship, and the TUM for subsequent funding through a HWP Ph.D. scholarship.

REFERENCES

(1) Fässler, T. F.; Hoffmann, S. D. *Angew. Chem., Int. Ed.* **2004**, *43*, 6242. *Angew. Chem.* **2004**, *116*, 6400.
(2) Schnepf, A.; Schnöckel, H. *Angew. Chem., Int. Ed.* **2002**, *41*, 3532. *Angew. Chem.* **2002**, *114*, 3682.
(3) Fässler, T. F. *Struct. Bonding (Berlin)* **2011**, *140*, 91.
(4) Scharfe, S.; Kraus, F.; Stegmaier, S.; Schier, A.; Fässler, T. F. *Angew. Chem., Int. Ed.* **2011**, *50*, 3630. *Angew. Chem.* **2011**, *123*, 3712.
(5) Rios, D.; Gillett-Kunnath, M. M.; Taylor, J. D.; Oliver, A. G.; Sevov, S. C. *Inorg. Chem.* **2011**, *50*, 2373.
(6) Lips, F.; Dehnen, S. *Angew. Chem., Int. Ed.* **2011**, *50*, 955. *Angew. Chem.* **2011**, *123*, 986.
(7) Kaskel, S.; Klem, M. T.; Corbett, J. D. *Inorg. Chem.* **2002**, *41*, 3457.
(8) Corbett, J. D. *Angew. Chem., Int. Ed.* **2000**, *39*, 670. Corbett, J. D. *Angew. Chem.* **2000**, *112*, 682.
(9) Ruck, M.; Dubenskyy, V.; Söhnel, T. *Angew. Chem., Int. Ed.* **2003**, *42*, 2978. *Angew. Chem.* **2003**, *115*, 3086.
(10) Wahl, B.; Erbe, M.; Gerisch, A.; Kloo, L.; Ruck, M. *Z. Anorg. Allg. Chem.* **2009**, *635*, 743.
(11) Spiekermann, A.; Hoffmann, S. D.; Fässler, T. F.; Krossing, I.; Preiss, U. *Angew. Chem., Int. Ed.* **2007**, *46*, 5310. *Angew. Chem.* **2007**, *119*, 5404.
(12) Moses, M. J.; Fettinger, J. C.; Eichhorn, B. W. *Science* **2003**, *300*, 778.
(13) King, R. B.; Zhao, J. *Chem. Commun.* **2006**, 4204.
(14) Stegmaier, S.; Fässler, T. F., manuscript submitted for publication.
(15) *X-AREA (Version 1.26)*; STOE & Cie GmbH: Darmstadt, 2004.
(16) *X-RED32 (Version 1.26)*; STOE & Cie GmbH: Darmstadt, 2004.
(17) *X-SHAPE (Version 2.05)*; STOE & Cie GmbH: Darmstadt, 2004.
(18) *XPREP (Version 6.14)*; Bruker Nonius: Madison, WI, 2003.
(19) *XS - Crystal Structure Solution - SHELXTL (Version 6.12)*; Bruker AXS: Madison, WI, 2001.
(20) Sheldrick, G. *Acta Crystallogr., Sect. A* **2008**, *64*, 112.
(21) *XL - Crystal Structure Refinement - SHELXTL (Version 6.12)*; Bruker AXS: Madison, WI, 2001.
(22) Gelato, L. M.; Parthe, E. *J. Appl. Crystallogr.* **1987**, *20*, 139.
(23) Spek, A. L. *Acta Crystallogr., Sect. A* **1990**, c34.
(24) Frisch, M. J.; et al. *Gaussian 09*, revision B.01; Gaussian, Inc.: Wallingford, CT, 2010.
(25) Schuchardt, K. L.; Didier, B. T.; Elsethagen, T.; Sun, L.; Gurumoorthi, V.; Chase, J.; Li, J.; Windus, T. L. *J. Chem. Inf. Model.* **2007**, *47*, 1045.
(26) Feller, D. *J. Comput. Chem.* **1996**, *17*, 1571.
(27) Dennington, R., II; Keith, T.; Millam, J.; Eppinnett, K.; Hovell, W. L.; Gilliland, R. *GaussView (Version 3.09)*; Semichem, Inc.: Shawnee Mission, KS, 2003.
(28) Becke, A. D. *J. Chem. Phys.* **1993**, *98*, 5648.
(29) Lee, C.; Yang, W.; Parr, R. G. *Phys. Rev. B* **1988**, *37*, 785.
(30) Weigend, F.; Ahlrichs, R. *Phys. Chem. Chem. Phys.* **2005**, *7*, 3297.
(31) Metz, B.; Stoll, H.; Dolg, M. *J. Chem. Phys.* **2000**, *113*, 2563.
(32) Glendening, E. D.; Reed, A. E.; Carpenter, J. E.; Weinhold, F. *NBO (Version 3.1)*.
(33) Barone, V.; Cossi, M. *J. Phys. Chem. A* **1998**, *102*, 1995.
(34) Cossi, M.; Rega, N.; Scalmani, G.; Barone, V. *J. Comput. Chem.* **2003**, *24*, 669.

(35) Jepsen, O.; Burkhardt, A.; Andersen, O. K. *The Stuttgart TB-LMTO-ASA Program (Version 4.7)*; Max-Planck-Institut für Festkörperforschung: Stuttgart, 1998.
(36) Barth, U. v.; Hedin, L. *J. Phys. C: Solid State Phys.* **1972**, *5*, 1629.
(37) Blöchel, P. E.; Jepsen, O.; Andersen, O. K. *Phys. Rev. B* **1994**, *49*, 16223.
(38) Larsson, A. K.; Stenberg, L.; Lidin, S. *Acta Crystallogr., Sect. B* **1994**, *50*, 636.
(39) Pani, M.; Merlo, F.; Fornasini, M. L. *Z. Anorg. Allg. Chem.* **2007**, *633*, 1581.
(40) Scharfe, S.; Fässler, T. F.; Stegmaier, S.; Hoffmann, S. D.; Ruhland, K. *Chem.-Eur. J.* **2008**, *14*, 4479.
(41) Wang, J.-Q.; Stegmaier, S.; Wahl, B.; Fässler, T. F. *Chem.-Eur. J.* **2010**, *16*, 1793.
(42) Hewaidy, I. F.; Busmann, E.; Klemm, W. *Z. Anorg. Allg. Chem.* **1964**, *328*, 283.
(43) Grin, Y.; Baitinger, M.; Kniep, R.; von Schnering, H. G. *Z. Kristallogr.-New Cryst. Struct.* **1999**, *214*, 453.
(44) Hoch, C.; Wendorff, M.; Rohr, C. *Acta Crystallogr., Sect. C* **2002**, *58*, i45.
(45) Gallmeier, J.; Schäfer, H.; Weiss, A. *Z. Naturforsch., B* **1969**, *24*, 665.
(46) Zhao, J.-T.; Corbett, J. D. *Inorg. Chem.* **1994**, *33*, 5721.
(47) Fässler, T. F.; Kronseder, C. *Z. Anorg. Allg. Chem.* **1998**, *624*, 561.
(48) Bobev, S.; Sevov, S. C. *Inorg. Chem.* **2000**, *39*, 5930.
(49) Bobev, S.; Sevov, S. C. *J. Am. Chem. Soc.* **2002**, *124*, 3359.
(50) Bobev, S.; Sevov, S. C. *Inorg. Chem.* **2001**, *40*, 5361.
(51) Echeverria, J.; Casanova, D.; Llunell, M.; Alemany, P.; Alvarez, S. *Chem. Commun.* **2008**, 2717.
(52) Gallucci, J. C.; Doecke, C. W.; Paquette, L. A. *J. Am. Chem. Soc.* **1986**, *108*, 1343.
(53) Bertau, M.; Wahl, F.; Weiler, A.; Scheumann, K.; Wörth, J.; Keller, M.; Prinzbach, H. *Tetrahedron* **1997**, *53*, 10029.
(54) Liu, S.; Lu, Y.-J.; Kappes, M. M.; Ibers, J. A. *Science* **1991**, *254*, 408.
(55) David, W. I. F.; Ibberson, R. M.; Matthewman, J. C.; Prassides, K.; Dennis, T. J. S.; Hare, J. P.; Kroto, H. W.; Taylor, R.; Walton, D. R. M. *Nature* **1991**, *353*, 147.
(56) Bürgi, H.-B.; Blanc, E.; Schwarzenbach, D.; Liu, S.; Lu, Y.-J.; Kappes, M. M.; Ibers, J. A. *Angew. Chem., Int. Ed. Engl.* **1992**, *31*, 640. *Angew. Chem.* **1992**, *104*, 667.
(57) Wunderlich, J. A.; Lipscomb, W. N. *J. Am. Chem. Soc.* **1960**, *82*, 4427.
(58) Tiritiris, I.; Schleid, T.; Müller, K.; Preetz, W. *Z. Anorg. Allg. Chem.* **2000**, *626*, 323.
(59) Döring, W.; Seelentag, W.; Buchholz, W.; Schuster, H. U. *Z. Naturforsch., B* **1979**, *34*, 1715.
(60) Yong, L.; Hoffmann, S. D.; Fässler, T. F. *Z. Anorg. Allg. Chem.* **2005**, *631*, 1149.